Innovative Approach to Pavement Rehabilitation Analysis and Design of Runway (R/W) 15L-33R at George Bush Intercontinental Airport (IAH) in Houston, TX

Corey J. Zollinger[1], D. G. Zollinger[2], P.E, Member ISCP, D.N. Little[3], P.E.[3], A. Godiwalla[4], P.E., R.P.S.

Introduction

In late 2003, the City of Houston determined Runway (R/W) 15L-33R at George Bush Intercontinental Airport/Houston (IAH) should be rehabilitated in order to provide an additional 20 years of useful life. The City required the Engineering Consultants to provide two possible pavement rehabilitation options one of which to include a PCC overlay or remove and reinstall the keel section. The existing runway was originally constructed under 3 different contracts. The original contract constructed the North 2440 m (sta 0+003 to sta 0+027) in 1968 and consisted of a 200 mm sand-shell sub-base with a 304 mm PCC slab which was later overlaid with a 457 mm PCC partially bonded overlay in 1976. At the same time, a 1220 m extension was added on the south end (sta 0+027 to sta 0+039) which consisted of a 533 mm PCC layer over a 152 mm asphalt treated sub-base.

The rehabilitation strategy proposed for this project was developed by using an innovative approach to interlayer stiffness in determining the existing condition of the runway, performing both fatigue and deflection analyses on the existing pavement structure for each section, and finally identifying pavement design criteria to configure each rehabilitation strategy. The fatigue analysis was not elaborate and was determined by the Layered Elastic Airport Pavement Design software (LEDFAA v1.3), taking into account damage by the critical stress imposed by each aircraft included in the runway traffic mix. Since LEDFAA does not consider the accumulation of permanent deformation in the subgrade under deflection imposed by each aircraft, deflection criteria was developed in order to give a more complete picture of what different rehabilitation options offer performance-wise. Deflection design criteria was formulated to prevent permanent deformation in the subgrade due to loads imposed by the heavy aircraft included in the runway traffic mix. Permanent deformation of this nature may lead to loss of support below the slab.

As greater demands are being placed on our airport systems by increasing traffic and loading, improved pavement rehabilitation analysis and design methods are needed to fully account for all factors manifest in the condition of the pavement. This paper presents an innovative approach to account for the many factors

[1] Graduate Research Assistant, Dept. of Civil Engineering, Texas A&M Univ., College Station, TX 77843-3135 email:czollinger@tamu.edu
[2] Associate Professor, Dept. of Civil Engineering, Texas A&M Univ., College Station, TX 77843-3135
[3] Professor, Dept. of Civil Engineering, Texas A&M Univ., College Station, TX 77843-3135
[4] Assistant Director of Aviation, Houston Airport System, P.O. Box 60106, Houston, TX 77205-0106

influencing concrete pavement stiffness regarding the design and analysis of rehabilitation alternatives. The approach described affords practitioners a tool to realistically take into account current pavement conditions and future traffic loadings.

Pavement Condition Assessment

The assessment of the pavement condition was done visually, destructively, and non-destructively. Visual inspection indicated that the North 2440 m could be divided into two segments: the North 915 m and the Middle 1525 m for rehabilitation purposes. In both of these sections, the course aggregate in the top 457 mm was a blend of limestone and gravel. It was evident that very little structurally related damage had developed in the middle 1525 m and the South 1220 m segments. However, it was clear the North 915 m had suffered significant cracking distress including longitudinal cracking and spalling of the transverse joints as noted in Figure 1. It was speculated based on the construction sequencing of this portion of the runway, the surface cracking was a result of reflective fatigue cracking from the original 304 mm layer into the present 457 mm surface layer. Most of this type of cracking, although extensive, was limited to the center 15.2 m of the runway.

Figure 1 Sample of Cracking Distress in the North 915 m.

The visual inspection also revealed a significant amount of deterioration of the pavement surface shown in Figure 2. The cause of this deterioration is not entirely clear but it is thought to be related in part to the extensive amount of milling that was carried out on the surface of the 457 mm partially bonded overlay after construction in order to meet the finished grade and profile. The North 2440 m had also suffered some spall damage characteristic of gravel concrete.

Figure 2 Surface Deterioration of the North 2440 m.

The non-destructive testing (NDT) that was performed with a 22,600 kg HWD Dynatest 8082 Falling Weight Deflectometer (Figure 3) specially designed for airfield pavements. Center plate, center of slab deflections are illustrated in Figure 4 for the entire runway length.

Figure 3 Dynatest 8082 FWD.

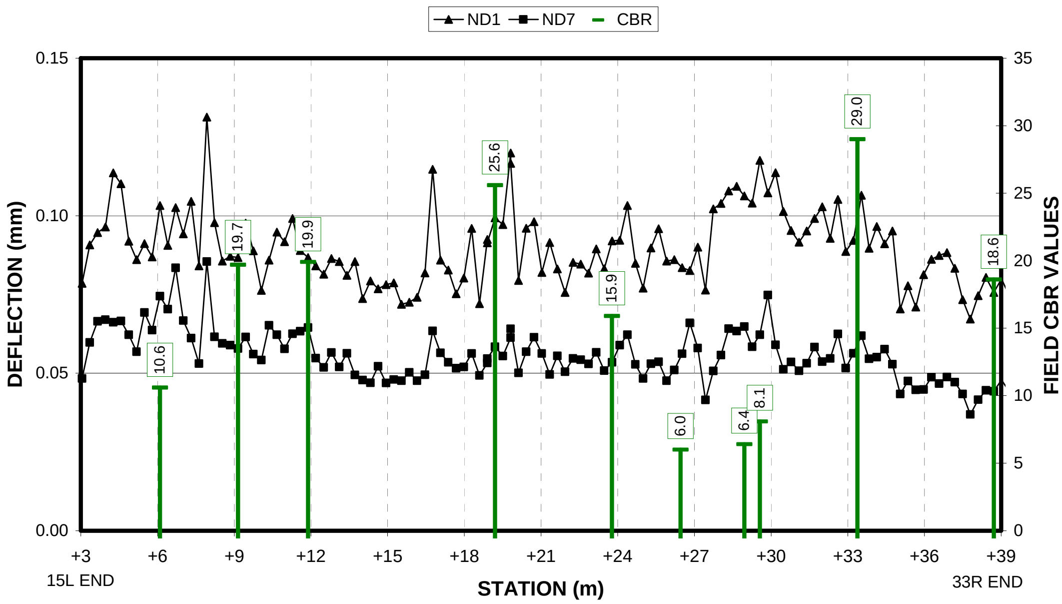

Figure 4 Runway 15L-33R (Centerline) Slab Centers Deflections.

The FWD deflection data was useful to determine several parameters related to the structural integrity of the 15L – 33R runway pavement listed as:

- Area of the deflected basin (BA) (L)
- Insitu radius of relative stiffness (RRS also referred to as ℓ value) (L)
- Effective slab thickness (h_e) (L)
- Dynamic foundation modulus (k value) (FL^{-2}/L)
- Joint load transfer efficiency (LTE) (%)

The BA is determined directly from the sensor deflection data recorded for the FWD (Ioannides 1990):

$$BA = \frac{SS}{2 * D_0}\left[D_0 + 2\left(D_1 + D_2 + ... + D_{j-1}\right) + D_j\right]$$

where

SS = Sensor spacing

D_i = Sensor deflection (i = 0 to j)

The determination of RRS is directly dependant upon the basin area but relies on a theoretical relationship developed from finite element (FE) analysis. The FE model used for this relationship is subsequently described. This analysis resulted in a relationship illustrated in Figure 5 which was used to determine the insitu RRS at each position where center of slab measurements were made. The RRS can also be defined as:

$$\ell = \sqrt[4]{\frac{E_c h^3}{12(1-\nu^2)k}}$$

where

E_c = Elastic modulus of the PCC layer (FL^{-2})

h		= Slab thickness (L)
υ		= Poisson's ratio
k		= Foundation modulus (FL^{-2}/L)

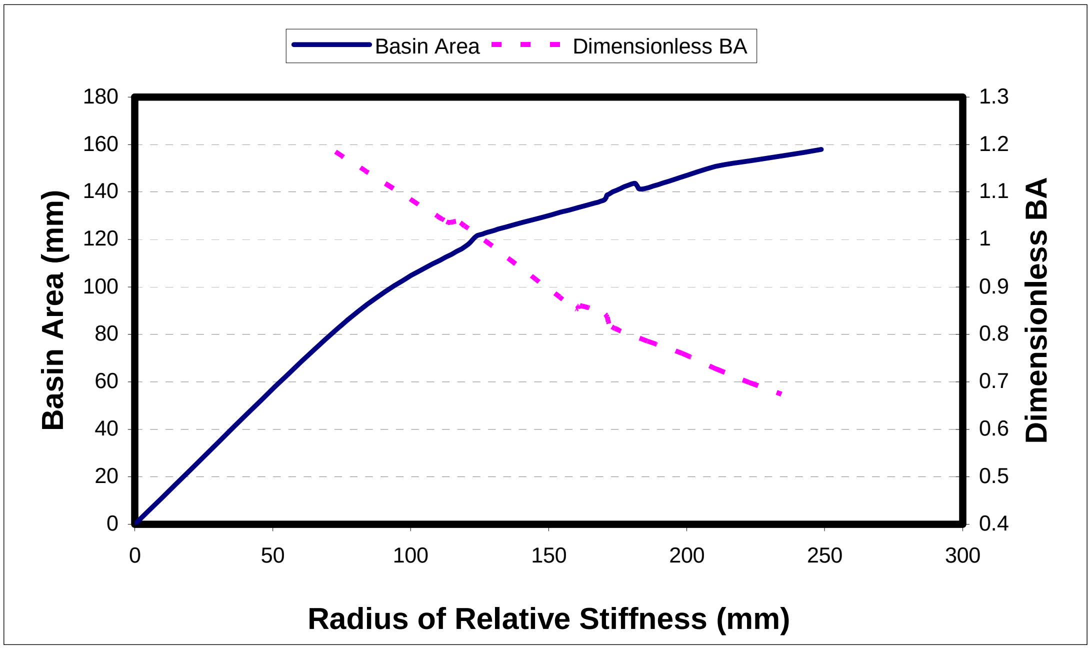

Figure 5 Basin Area – RRS Relationship.

The basin area was also presented for design purposes in a dimensionless form by dividing it by the RRS, providing greater dimensional utility in the analysis. Rearranging the relationship for RRS, the effective slab thickness was determined as:

$$h_e^3 = \frac{12\left(1-\nu^2\right)k}{E_c}\ell_e^4$$

E_c in these determinations were based on destructive compression tests on cores taken from the runway concrete. The h_e parameter is very useful as comparison to the measured in place thicknesses and an indicator of the structural condition of the in place pavement system. The RRS along with the center plate deflections are also useful to determine the foundation modulus of the subgrade. Since the deflection data is associated with a rather high frequency loading cycle, the resulting calculation is assumed to result in a dynamic foundation modulus (k_{dyn}) as (Ioannides 1990):

$$k_{dyn} = \frac{w_o^* P}{w_o \ell^2}$$

where

P	= Wheel load (F)	
w_0	= Center plate deflection (L)	
ℓ	= Radius of relative stiffness (L)	
w_0^*	$= \frac{1}{8}\left[1+\left(\frac{1}{2\pi}\right)\left(\ln\left(\frac{a}{2\ell}\right)+\gamma-1.25\right)\left(\frac{a}{\ell}\right)^2\right]$	(center of slab loading)

The static modulus of subgrade reaction was approximated from soil classification, field CBR testing, field DCP testing, and laboratory resilient modulus testing. A reasonable approximation of the static k-value for this soil based on this data was between 32.6 to 43.3 kPa/mm. Since no theoretical relationships between the subgrade foundation modulus and resilient modulus exist, relating these two parameters and the subgrade models upon which they are derived is always a challenge for designers. Nonetheless, assuming an equivalent deflection between the two theories, a useful relationship can be derived. Consequently, it was determined that for a soil MR of 7300 psi, a static k value of 35.4 kPa/mm could be assigned to it. The corresponding dynamic k-value, which can reasonably be applied to the runway where traffic loads are normally transient with a relatively short dwell time, greater than about 0.1 seconds, ranged between 65.1 to 86.8 kPa/mm.

Another important parameter is the deflection based load transfer efficiency of the transverse joints which is found from the loaded and unloaded deflections across the joint:

$$LTE = \frac{\delta_{unloaded}}{\delta_{loaded}} x100$$

This parameter is a useful indicator of the ability of the dowel bars and the pavement system to transfer load across the joint to the adjacent slab. The average LTE for the Middle and South sections was 77% but joints manifesting LTE less than 70% were considered for retro-fitting to restore the load transfer capability of those joints. Table 1 summarizes the NDT parameters noted above for the three sections of R/W 15L and 33R. The calculation of the interlayer friction coefficient (μ) will be explained later in the paper.

Table 1 Average Values of NDT Parameters of R/W 15L-33R.

Parameter	North 915 m	Middle 1525 m	South 1220 m
Area (cm)	148.3	139.0	132.9
RRS (cm)	206.1	179.0	162.1
h_e (cm)	61.2	50.9	44.4
Dynamic k value (kPa/mm)	79.5	106.3	120.4
Interlayer friction coefficient	50.4	21.0	
LTE (%)	77	77	77
# of Joints < 70%		7	8

A variety of destructive testing was carried out on samples from selected PCC cores listed in Table 2. The tests consisted of compressive and split tensile testing and testing of the bond strength across the interface of the 457 and 304 mm layers. Three of the five PCC core samples delivered for testing taken from the North 2440 m were broken at the interface suggesting the interfacial strength to be low and that only a few areas of the interlayer are well bonded. Two of the intact cores were cored horizontally at the interface and tested in a split tensile mode. The ASTM standards followed for this testing are also listed in Table 2.

Table 2 Destructive Test Results of Core Samples Obtained from R/W 15L-33R.

Core Sample	Station	Layer (in)	Compressive Strength (f'_c) (kPa) ASTM C 39	Elastic Modulus (E_c) (kPa) ASTM E111	Split Tensile Strength (f_t) (kPa) ASTM C 496	Interfacial Bond Strength (kPa) ASTM C 496
C-2	20+00	18		48263299		
		12		27579028		
C-6	39+00	18			4516	4854
		12			5619	
C-9	63+00	18	45974	32060620 *		
		12	74677	40885909 *		
C-12	81+00	18			5474	4806
		12			4875	
C-14	95+00	21	52545	34335890 *		

* E_c calculated from $4.73\, f'_c{}^{0.5}$

Two core specimens were tested according to ASTM E 111 for the elastic modulus by monitoring stress and strain within the elastic range of the concrete. The results of that testing are shown in Figure 6. The modulus values for core C-9 were used to determine the values listed in Table 1.

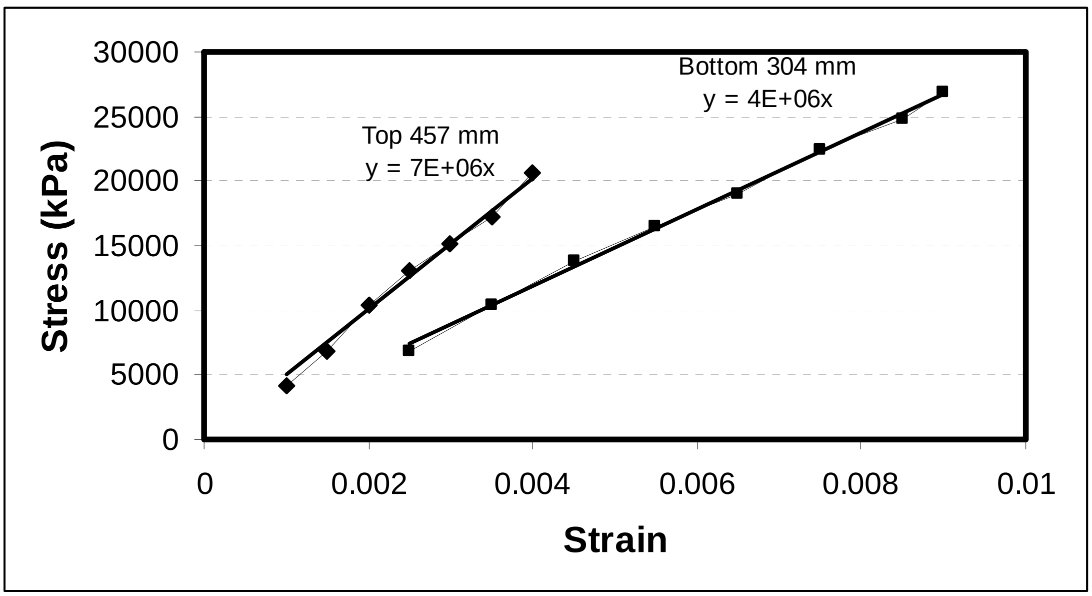

Figure 6 Stress-Strain Data for Elastic Modulus Testing.

Load and Deflection Analysis

Concrete slab load and deflection analysis was performed using ISLAB2000. This analysis was based upon assuming 1) a Westergaard subgrade; 2) that strain levels in the subgrade and concrete layers are within the elastic range and 3) that shear stresses in the vicinities of the loaded area are not significant (i.e. that medium thick plate theory applies). The load effects of the aircraft gear configurations in the mix (Table 3) were analyzed with respect to slab deflections and stresses computed at the critical slab location for maximum response and with respect to the transverse variability of the nose and main gears about the center position of the runway.

Table 3 Aircraft Types and Loading Data.

Aircraft Type	Gross Wt (kg)	Annual Departures	Gear Load (kg)	Tire Pressure (kPa)	Wheel Load (kg)
DC-8	162503	119	77133	1344	19284
DC-9-30	49477	36	23485	1048	5871
DC-9-50	51974	71715	26286	1172	13143
DC-10-30	272352	1325	129274	1344	32318
DC-10-30-BELLY	272352	1325	46266	1055	23133
B-727	86472	7765	37058	1103	18529
B-737-300	59010	43580	28009	1386	14005
B-737-800	78528	40470	37274	1386	18637
B-747-400	396272	54	188093	1379	4275
B -747-200	378115	488	179475	1379	26725
B-757	113480	251	53864	1241	13466
B -777-200 C*	327730	5389	155559	1503	25926
A320	64003	1032	32318	1379	16159
A340-200/300	254195	1916	99064	1420	24766
A340-200/300 Belly	254195	1916	43182	1089	21591
Fokker F100	45392	143	21546	979	10773
Dual Tan - 400	181568	90	95493	1379	23873
Dual Tan - 400	226960	24	95493	1379	23873
A380-800	562407	24	160339	1462	26723

* Design Aircraft

The ISLAB2000 (2000) analysis also included consideration for the degree of bonding between the 457 and 304 mm concrete layers. For each aircraft, ISLAB generated data to define the relationships between radius of relative stiffness (RRS), dimensionless stress, and deflection. Each relationship was developed by changing the layer thickness or the degree of bonding (which were represented, subsequently described, with different effective thicknesses of the slab) and recording the stress or deflection for each case. The following equations were used in developing the relationships:

Radius of Relative Stiffness (RRS or ℓ):

$$\ell = \sqrt[4]{\frac{E_c h_e^3}{12(1-\nu^2)k}}$$

Effective thickness for fully bonded layers as (Ioannides et al. 1992):

$$h_{e-b} = \left\{ h_1^3 + \frac{E_2}{E_1} h_2^3 + 12 \left[\begin{array}{l} \left(x_{na} - \frac{h_1}{2} \right)^2 h_1 \\ + \frac{E_2}{E_1} \left(h_1 - x_{na} + \frac{h_2}{2} \right)^2 h_2 \end{array} \right] \right\}^{1/3}$$

$$x_{na} = \frac{E_1 h_1 \frac{h_1}{2} + E_2 h_2 \left(h_1 + \frac{h_2}{2} \right)}{E_1 h_1 + E_2 h_2}$$

Effective thickness for unbonded layers (Ioannides et al. 1992):

$$h_{e-u} = \left[\left(h_1^3 + \frac{E_2}{E_1} h_2^3 \right) \right]^{1/3}$$

Dimensionless Stress:

$$s_{e-i}^* = \frac{\sigma h_{e-i}^2}{P}$$

Dimensionless Deflection:

$$d^* = \frac{\delta k \ell_{e-i}^2}{P}$$

where

E_c	= Elastic modulus of the PCC layer (FL^{-2})
h_{e-b}	= Effective thickness of the bonded PCC layers (L)
h_{e-u}	= Effective thickness of the unbonded PCC layers (L)
h_{e-p}	= Effective thickness of partially bonded PCC layers (L)
h_{e-i}	= h_{e-b}, h_{e-u}, h_{e-p} as the case may be
υ	= Poisson's ratio
k	= Foundation modulus (FL^{-2}/L)
E_1 or E_2	= Elastic modulus for layer 1 or 2 (FL^{-2})
h_1 or h_2	= Thickness for layer 1 or 2 (L)
s_{e-i}^*	= Effective dimensionless stress
σ	= Recorded stress from ISLAB2000 (FL^{-2})
P	= Wheel load (F)
d^*	= Dimensionless deflection
δ	= Recorded deflection from ISLAB2000 (L)
ℓ_{e-i}	= Radius of relative stiffness (L)
x_{na}	= Neutral axis distance from top of layer 1 (L)

The above expressions for effective thickness are also involved in the determination of the effective slab thickness for partially bonded conditions (h_{e-p}) between the slab and the stabilized layer below in which it is assumed that frictional slippage between these layers under load even represents the interlayer structural restraint. Whether the restraint or the variation of it between the layers is due to friction or chemical cohesion the determination of this restraint is referred to in this paper as the degree of bonding denoted as "x" (which ranges between 0 and 1) and is formulated as:

$$h_{e-p} = (1-x)\,h_{e-u} + (x)\,h_{e-b} \qquad (1)$$

Coincidentally, the h_e term calculated in Table 1 is equivalent to h_{e-p}; from rearrangement of equation (1) the degree of bonding can be assessed as:

$$x = \frac{h_{e-p} - h_{e-u}}{h_{e-b} - h_{e-u}} \qquad (2)$$

The prominence of the degree of bonding (x) parameter in design addressing partially bonded behavior necessitates its determination being predicated upon FWD data.

Figure 7 depicts the relationships between the partially bonded and unbonded effective thicknesses and stresses; using simple proportioning, the effective partially bonded stress (σ_{e-p}) can be found as:

$$\sigma_{e-p} = \sigma_e \left[\frac{2h_{e-u}}{h_{e-p}} - 1 \right] \qquad (3)$$

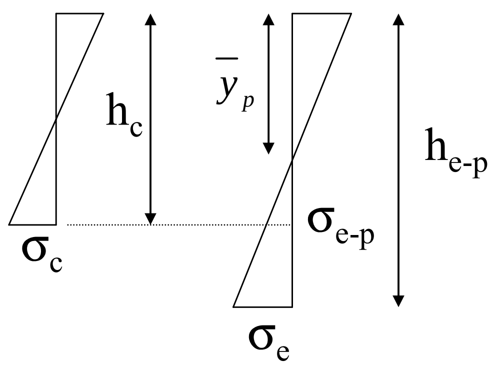

Figure 7 Unbonded and Partially-Bonded Transformed Section of a Concrete Slab.

In order to formulate a relationship to the interlayer friction coefficient (μ), the effective partially bonded stress (σ_{e-p}) is equated to the difference between the unbonded stress (σ_{e-u}) and the frictional stress (τ) at the bottom of the slab as:

$$\sigma_{e-p} = \sigma_{e-u} - \tau = \frac{s^*_{e-u} P}{h^2_{e-u}} - \mu \left[\frac{h_c}{12} + \sigma_v \right] \qquad (4)$$

Equations 3 and 4 can be rearranged to develop an expression for μ as:

$$\mu = \frac{\sigma_{e-u} - \sigma_T \left[\frac{2h_{e-u}}{h_{e-p}} - 1 \right]}{\frac{h_c}{12} + \sigma_v} \qquad (5)$$

where

σ_T = $\frac{s^*_{e-i} P}{h^2_{e-i}}; s_{e-i} = a + b\ell_{e-i} + c\ell^2_{e-i}$ (for FWD plate loading)

P = Applied FWD load (F)

a, b, c = 0.0006, 0.0403, and -0.0002 (from FEA with ISLAB200 for FWD plate loading)

h_c = Insitu concrete slab thickness (L)

σ_v = Load induced vertical pressure at partially-bonded interface (FL^{-2}) ($\approx$ 4.82 kPa)

Using the expressions (2) and (5), the degree of bonding (as defined above) and the interlayer coefficient of friction can be back-calculated for each location of FWD testing. The results of these back calculations are shown in Figure 8 and suggest that the degree of bonding can be related to the coefficient of friction (μ). To that end, the following relationship is proposed:

$$x = e^{-\left(\frac{A}{\mu}\right)^B} \qquad (6)$$

Where

A $= e^{\frac{1.232-0.065\mu}{B}}$

B $= -\left(0.039y^2\right)$

y = Ln (μ)

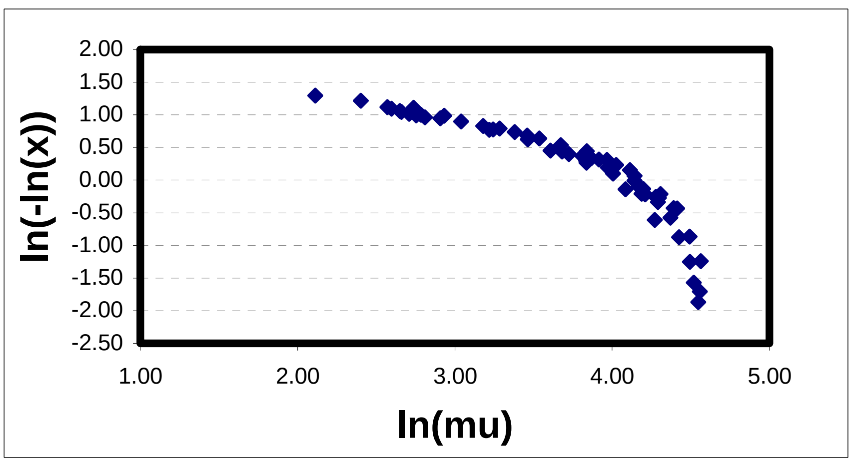

Figure 8 Relationship between Backcalculated Values of μ and Degree of Bond.

The back calculated degree of bonding ranged from 0 to 0.83 but several locations was zero. In terms of design, research has indicated (where chemical cohesion was assumed to be minimal) that the parameter μ varies as of function of the subbase material type (for granular bases μ ≈ 1.5, asphalt concrete bases ≈ 3 to 6, and cement stabilized bases ≈ >15) (Wimsatt et al. 1987). The evaluation of the relationship between these parameters based on the back calculations shown above using the collected FWD data from R/W 15L-33R significant because of the range of μ that equation (6) encompasses makes it applicable to other design scenarios. Consequently, equation (6) can be used as a design tool to represent the interlayer structural restraint from a frictional interaction perpective between the concrete layers of the North 915 m feet and Middle 1525 m sections.

In addition to development of the dimensionless stress and deflection curves, the ISLAB2000 program was also used to evaluate the effects of aircraft wander on the pavement deflections as previously noted. Figure 9 illustrates deflections induced on the pavement at the critical design location (located 5.58 m from the runway centerline positioned along the transverse joint) as the gear load for the Boeing 777 aircraft was varied within a 3.2 m standard deviation.

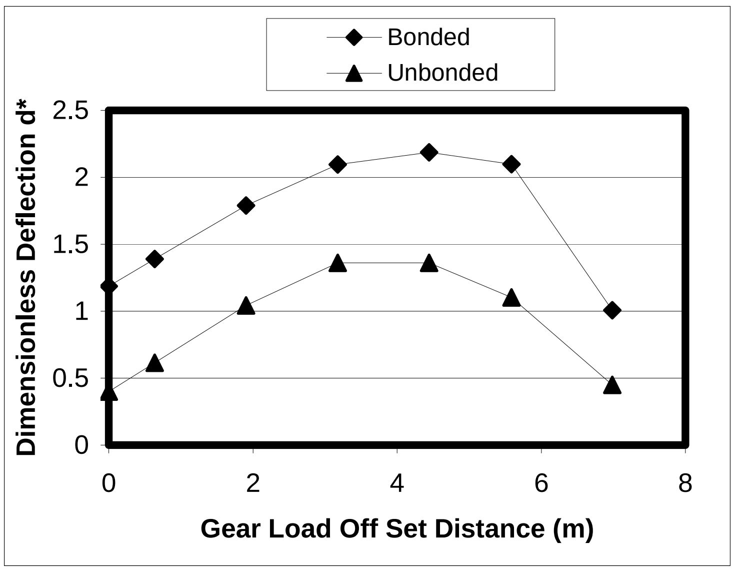

Figure 9 Distribution of Deflection at the Design Location

Pavement Design Criteria

The Layered Elastic Airport Pavement Design (LEDFAA v 1.3) program was used to determine the design thickness of an un-bonded PCC overlay over a 304 mm concrete slab for a design life of 20 years. Using the aircraft mix as previously discussed and an SCI of 80 the overlay thickness determined by LEDFAA was 457 mm for the design aircraft Boeing 777. The LEDFAA analysis indicates that slab thickness of 457 mm will satisfy the fatigue criteria for the design aircraft B 777. In addition to the fatigue criteria, slab deflection criteria were established to protect the subgrade from excessive vertical stresses that induce permanent deformation in the subgrade.

Pavement Deflection Criteria. The maximum deflection allowed was based on the subgrade type and its elastic characteristics relative to the maximum strain associated with its elastic range of strain. In like manner, the maximum allowable stress that can be tolerated by the native subgrade is based on the elastic-plastic characteristics of the subgrade. These concepts are illustrated in Figure 10, which is a typical, generic plot of stress v. strain under monotonic loading for a soil. Note that up to a stress of about one-half of the ultimate, unconfined compressive stress (UCCS) at failure, the stress-strain response is linear; and if a cyclic load or stress were applied up to about 1/2 UCCS, the strain is typically fully recoverable for each application of load or stress. The rate of permanent deformation accumulation is assumed to occur at an unacceptable rate if the cyclic stress exceeds about 1/2 UCCS. At this point each load or stress cycle results a permanent or non-recoverable strain. Over time and load, this cumulative strain builds resulting in a loss of support under the slab. Loss of subgrade support is a parameter that may affect pavement performance and is a causative factor related to joint faulting and corner cracking.

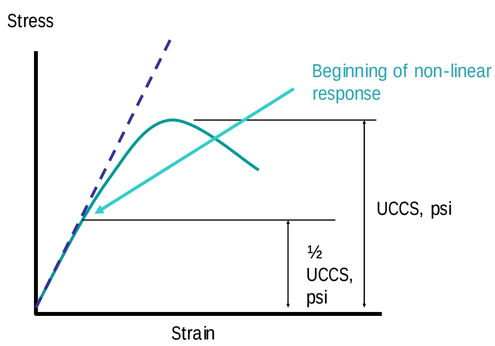

Figure 10 Typical Stress-Strain Response in Subgrade Soil.

Based on this approach, the pavement structure was designed so that stresses induced in the subgrade under traffic loading would not exceed 0.5 of the UCCS. Soil classification can be used to approximate the compressive strength of the subgrade. Table 4 was used as a general guide (Huang 2004).

Table 4 Approximate Subgrade Parameters Based on Soil Classification.

General Classification	Approximate Resilient Modulus at a Deviatoric Stress of 41 kPa	Approximate Unconfined Compressive Strength, kPa
Stiff, fine-grained	85150	228
Medium, fine-grained	52952	159
Soft, fine-grained	20822	90
Very soft, fine-grained	6895	41

Based on the general classification of the subgrade soil and in situ CBR and dynamic cone penetrometer data (DCP), the native subgrade was reasonably assigned a design resilient modulus of approximately 51711 kPa and a UCCS of approximately 138 kPa to 172 kPa. This approximation is supported by field FWD testing where the native subgrade soil resilient modulus was back-calculated from deflection data. Since the subgrade modulus is back-calculated to match the extreme sensor in the FWD configuration, the stress state in the subgrade that causes the deflection at the extreme sensor is very low, typically much lower than the 41 kPa design deviatoric stress. Therefore, the design resilient modulus is normally between one-third to one-fifth of the back-calculated modulus from the FWD data.

As a final validation of resilient properties of the native subgrade, resilient modulus testing was performed following AASHTO method 307-02. The design resilient properties based on these tests were in reasonable agreement with the approximated values. Based on this approach, one would require that subgrade stresses induced by aircraft traffic loads would not exceed about 69 to 83 kPa.

Shear Stress Criteria. Other criteria were based on concerns of the City of Houston relative to the load induced horizontal shear stresses being significant near the surface of the pavement at the overlay interface. Finite element analysis was used to assess the impact of these shear stresses. Analysis was performed for shear stress distributions under 11,340 kg and 34,020 kg wheel loads for 51 mm and 152 mm thick overlays. It was determined the shear stresses induced (including those by braking forces) at the interface of the 51 mm overlay are not likely to exceed the shear strength of the PCC, assumed to be approximately 20 percent of the compressive strength (Troxell et al. 1968). However, with a loss of bond, the shear stresses may exceed the shear strength at the interface of the thinner overlay under the heavier wheel load.

Elaborating further, the impact of a discontinuity between the proposed overlay and the existing PCC pavement (Figure 11), a braking aircraft imparts a shearing stress where the discontinuity magnifies the stress intensity at the tip of the discontinuity. The shear stress intensity factor, K_{II} was approximated based on the imposed shear stress (calculated using the finite element model) and the relative geometry of the crack (size and shape) compared to the relative geometry of the pavement.

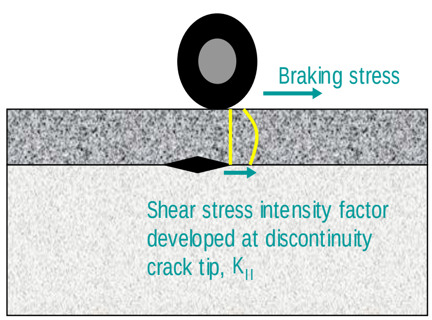

Figure 11 Stress Intensity at Discontinuity between Overlay and Existing Pavement.

Based on this analysis of the shear stress intensity factor, the critical shear stress, $\tau_{critical}$ that would cause the discontinuity to become unstable was calculated from fracture mechanics as:

$$\tau_{critical} = \frac{K_{II}}{\sqrt{\pi a}}$$

where K_{II} varied as a function of load and geometry and 'a' is one-half the length of the discontinuity. Shear stresses were calculated for static and braking wheel loads for different overlay thicknesses and discontinuity lengths. The induced stresses were compared with the critical shear stresses and are summarized in Tables 5 and 6.

Table 5 Critical Shear Stresses assuming a 304 mm Discontinuity at the Overlay-Interface.

Overlay Thickness, mm	Static Shear Stress at Crack Tip, kPa	Shear Stress at Crack Tip with Braking, kPa	Critical Shear Stress, kPa
51	2551	3571	2344
102	414	1793	2344
152	207	896	2344
203	69	303	2344

Table 6 Critical Shear Stresses assuming a 608 mm Discontinuity at the Overlay-Interface.

Overlay Thickness, mm	Static Shear Stress at Crack Tip, kPa	Shear Stress at Crack Tip with Braking, kPa	Critical Shear Stress, kPa
51	3571	4999	2344
102	2523	3530	2344
152	1241	1737	2344
203	69	303	2344

Comparison of the stress data listed in Table 5 and 6 to the critical stress (i.e. concrete strength), a 152 mm PCC overlay was sufficient to retard the progression of at 608 mm discontinuity, and a 76 mm PCC overlay was sufficient to retard the progression of a 304 mm discontinuity.

Deflection Variability

The approach taken to consider deflection variability was by accounting for the factors influencing slab deflection and determining the deflection variance due to them. Relative to slab deflection, the following factors affect variability:

- Modulus of elasticity, E_c
- Subgrade k value
- Interlayer friction, μ
- Load transfer efficiency, LTE

The total deflection variance is equivalent to the sum of the individual variances. The deflection variance (Var [δ]) is useful to determine a measured level of reliability against slab failure due to permanent subgrade deformation through the following expression:

$$\delta_{Design} = \alpha\bar{\delta} + z_R\left(SD_\delta\right) \qquad (7)$$

where

δ_{Design} = Design deflection (L)

$\overline{\delta}$ = Mean deflection (L)

SD_{δ} = Deflection standard deviation (L) = $\sqrt{Var[\delta]}$

z_R = Normal standard deviate (reliability factor)

α = Aircraft wander factor

Assuming the deviation of slab deflection (δ) at the critical load location on the slab is normally distributed about the mean, z_R can be selected for a given level of reliability from a normal standard deviate table (i.e. for a 95% reliability $z_R = 1.645$). The contribution of each factor noted above to the total variance is based the factor coefficient of variation (COV) which is equal to the standard deviation divided by the mean. Given the COV, the variances of each factor can be found as:

$$Var[X_i] = \left(COV[X_i] \cdot \overline{X}_i\right)^2$$

The expression for the total deflection variance (Var[δ]) is found from the first order – second moment method as (Montgomery and Runger 2003):

$$Var[\delta] = \sum_i^n \left(\frac{\partial \delta}{\partial X_i}\right)^2 Var[X_i] + \sum_i^n \sum_j^n \left(\frac{\partial \delta}{\partial X_i}\right)\left(\frac{\partial \delta}{\partial X_j}\right) \rho_{\substack{i,j \\ i \neq j}} \qquad (8)$$

where

X_i = E_c, k, μ, and LTE

$\rho_{i,j}$ = Correlation parameter (= 0, for the given list of X_i)

Aircraft wander is another parameter that affects deflection variance but since it is associated with repeated load behavior, its affect in equation (7) is reflected in the aircraft wander factor (α - which varies between zero and 1.0 in equation 7). As previously noted, studies (Huang, 2004) of aircraft wander suggest the standard deviation of wander may be as high as 3.2 m for a runway facility but as the standard deviation decreases, the wander factor increases. Given the standard deviation of the wander, α can be calculated as shown in Table 7:

Table 7 Aircraft Wander Factor for B-777 Aircraft and SD = 1 m

z_R	Weight	Centerline Distance (m)	Deflection (mm)	Weighted Deflection	Aircraft Wander Factor
0.5	0.191462	5.3	4.3	1.653	
1	0.149882	4.8	4.1	0.621	
2	0.135905	4.0	3.8	0.518	
3	0.0214	2.9	3.2	0.068	
4	0.001318	1.9	2.6	0.003	
			∑	2.864	0.66

Note: a mean deflection of 4.368 mm was used for the calculation of α.

Rehabilitation Strategy

In the development of rehabilitation alternatives for R/W 15L – 33R, the level of reliability was applied equivalently across all alternatives. Due to the satisfactory performance of the South 1220 m, this section of the runway was used to establish the minimum level of reliability for rehabilitation alternative development even though its effective thickness is only approximately 80% of the actual slab thickness. Maintaining a subgrade stress of 69 kPa, the South section is currently performing at 97% reliability.

The back calculation analysis of the middle 1525 m suggests that this section is behaving as a 457 mm unbonded slab – which in one respect (50% level of reliability) eliminates the need for an overlay. The analysis for rehabilitation was carried out at a dynamic k value of 68.9 kPa/mm which is approximately double the static k value. Values of this parameter and the aircraft wander factor (=0.8) were conservatively selected for design purposes which may render some bias in the final results. Nonetheless, the level of these parameters is considered to be indicative of the conditions the runway will be performing under in the future. On this basis, a deflection analysis of the pavement was carried out to assess the adequacy of the existing pavement structure at different reliabilities, LTE's, and overlay thicknesses. Improvement in LTE was considered in the development of the rehabilitation strategy from the perspective that added assurance against the development of excessively low LTE over the next 20 years should be provided.

A variety of rehabilitation options depicted in Figure 12 were recommended to the City of Houston where each option provides an equal level of performance. The minimum bonded concrete overlay (BCO) of 76 mm is governed by horizontal shear stress criteria.

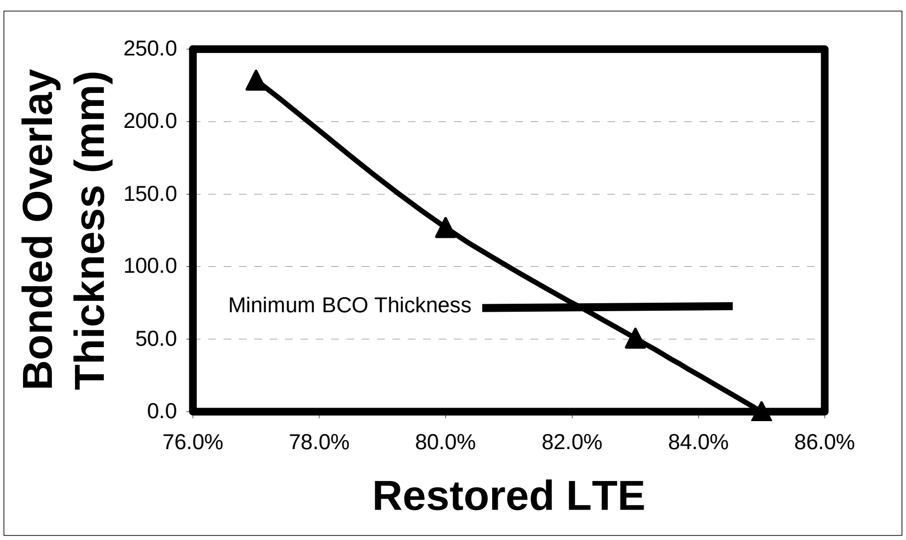

Figure 12 BCO Design Thickness vs. Improved LTE

- Option #1: Involves improvement of the LTE from an average of 77% to 85%, and a 76 mm mill and replacement of the existing pavement surface.
- Option #2: Involves improvement of the LTE to 83%, a 50 mm overlay is required due to horizontal shear stress levels, and the required depth of milling would only need to be 25 mm.
- Option #3: Involves improvement of the average LTE to 80% and a 127 mm BCO with no milling required.
- Option #4: Involves no improvement of LTE and a 230 mm BCO with no milling required.

The North 915 m section has been previously analyzed using the LEDFAA program. Using the deflection criteria at 95% reliability, an average LTE of 85%, it was determined that a 533 mm slab thickness is needed for the reconstruction of the runway keel area.

Conclusions

The rehabilitation strategy developed for this project was formulated by evaluating the existing condition of the runway, performing both fatigue and deflection analyses on the existing pavement structure for each section, and finally identifying pavement design criteria. These analysis methods were able to account for variable layer bonding ranging from completely un-bonded to fully bonded layers between the PCC overlay and existing PCC layers affecting pavement stiffness. These analysis methods also took into account variables affecting pavement stiffness including pavement thickness, interlayer friction, dowel bar size spacing, and load transfer efficiency. In this manner a variety of options were afforded the City of Houston providing an equivalent level of performance.

References

Huang, Y.H. (2004). *Pavement Analysis and Design*, 2^{nd} Ed., Pearson Prentice Hall, Upper Saddle River, NJ.

"ISLAB2000 –Finite Element Analysis Program for Rigid and Composite Pavements" User's Guide, ERES Consultants, 2000

Ioannides, A.M. (1990). "Dimensional Analysis in NDT Rigid Pavement Evaluation." Journal of Transportation Engineering, Vol. 116, No. 1, pp. 23-26.

Ioannides, A.M., Khazanovich, L., and Becque, J.L. (1992). "Structural Evaluation of Base Layers in Concrete Pavement Systems." Transportation Research Record 1370, Transportation Research Board, Washington, D.C., pp.20-28.

Montgomery, D.C., and Runger, G.C. (2003). *Applied Statistics and Probability for Engineers*, 3^{rd} Ed., Wiley, New York

Troxell, G.E., Davis, H.E., and Kelly, J.W. (1968) *Composition and Properties of Concrete*, 2^{nd} Ed., McGraw-Hill, New York.

Wimsatt, A.W., McCullough, F.B., and Burns, N.H. (1987). *Methods of Analyzing and Factors Influencing Frictional Effects of Subbases*, Report 459-2F, Center For Transportation Research, Austin, TX.